Published in final edited form as:
Sci Signal. ; 7(315): ra22. doi:10.1126/scisignal.2005025.

KCNQ1, KCNE2, and Na+-Coupled Solute Transporters Form Reciprocally Regulating Complexes that Affect Neuronal Excitability

Geoffrey W. Abbott[1,2,*], **Kwok-Keung Tai**[1], **Daniel Neverisky**[1], **Alex Hansler**[3], **Zhaoyang Hu**[1], **Torsten K. Roepke**[4,†], **Daniel J. Lerner**[4,#], **Qiuying Chen**[3], **Li Liu**[5], **Bojana Zupan**[3,¶], **Miklos Toth**[3], **Robin Haynes**[6], **Xiaoping Huang**[7], **Didem Demirbas**[7], **Roberto Buccafusca**[7], **Steven S. Gross**[3], **Vikram A. Kanda**[3,‡], and **Gerard T. Berry**[7,‡]

[1]Bioelectricity Laboratory, Department of Pharmacology, School of Medicine, University of California, Irvine, CA, USA

[2]Department of Physiology and Biophysics, School of Medicine, University of California, Irvine, CA, USA

[3]Department of Pharmacology, Cornell University, Weill Medical College, New York, NY, USA

[4]Department of Medicine, Cornell University, Weill Medical College, New York, NY, USA

[5]Department of Pathology, Taub Institute for Research on Alzheimer's Disease, Columbia University, New York, NY, USA

[6]Department of Pathology, The Manton Center for Orphan Disease Research, Division of Genetics and Genomics, Boston Children's Hospital, Harvard Medical School, MA, USA

[7]Department of Medicine, The Manton Center for Orphan Disease Research, Division of Genetics and Genomics, Boston Children's Hospital, Harvard Medical School, MA, USA

Abstract

[*]Address correspondence to: Dr. Geoffrey W. Abbott, 356A Med Surge II, Department of Pharmacology, School of Medicine, University of California, Irvine, CA, 92697, USA; abbottg@uci.edu.
[†]present address: Clinic for Cardiology and Angiology, Charite University-Medicine Berlin 10117 Berlin, Campus Mitte and Experimental and Clinical Research Center, Max Delbrueck Center for Molecular Medicine Berlin, Germany;
[#]present address: Tyrx Inc., Monmouth Junction, New Jersey, USA;
[¶]present address: Department of Psychology, Vassar College, Poughkeepsie, NY, USA
[‡]these authors contributed equally

Supplementary Material

Fig. S1. Mouse motor function and activity assays
Fig. S2. *Kcne2* deletion alters choroid plexus epithelium cell size and shape
Fig. S3. SMIT1, NKCC1 and KCNQ1 expression in choroid plexus and kidney
Fig. S4. KCNQ1 function with and without transporter coexpression
Fig. S5. Functional effects of SMIT2 interaction with KCNQ1-KCNE2
Table S1. CSF mass spectrometry.

Author contributions: All authors except D.J.L., M.T., G.T.B. and S.S.G. performed experiments. G.W.A., A.H., Z.H., Q.C., T.K.R., L.L., B.Z., M.T., S.S.G., D.J.L., D.D., X.H., R. H., R. B., G.T.B. and V.A.K. contributed to experimental design and/or data analysis. G.W.A. prepared the figures and wrote the manuscript; all authors edited the manuscript.

Competing interests: The authors declare that they have no competing interests.

Materials availability: An MTA is required by Harvard Medical School for the *Slc5a3*$^{-/-}$ mice.

Na^+-coupled solute transport is crucial for the uptake of nutrients and metabolic precursors, such as *myo*-inositol, an important osmolyte and precursor for various cell signaling molecules. Here, we found that various solute transporters and potassium channel subunits formed complexes and reciprocally regulated each other in vitro and in vivo. Global metabolite profiling revealed that mice lacking KCNE2, a K^+ channel β subunit, showed a reduction in the *myo*-inositol concentration in cerebrospinal fluid (CSF) but not in serum. Increased behavorial responsiveness to stress and seizure susceptibility in *Kcne2*$^{-/-}$ mice were alleviated by injections of *myo*-inositol. Suspecting a defect in *myo*-inositol transport, we found that KCNE2 and KCNQ1, a voltage-gated potassium channel α subunit, colocalized and coimmunoprecipitated with SMIT1, a Na^+-coupled *myo*-inositol transporter, in the choroid plexus epithelium. Heterologous coexpression demonstrated that *myo*-inositol transport by SMIT1 was augmented by coexpression of KCNQ1 but inhibited by coexpression of both KCNQ1 and KCNE2, which form a constitutively active, heteromeric K^+ channel. SMIT1 and the related transporter SMIT2 were also inhibited by a constitutively active mutant form of KCNQ1. The activity of KCNQ1 and KCNQ1-KCNE2 were augmented by SMIT1 and the glucose transporter SGLT1, but suppressed by SMIT2. Channel-transporter signaling complexes may be a widespread mechanism to facilitate solute transport and electrochemical crosstalk.

Introduction

Voltage-gated potassium (Kv) channel pore-forming α subunits form complexes with a range of ancillary (β) subunits, such as the single-transmembrane domain proteins encoded by the *KCNE* gene family (Fig. 1A), leading to various channel subunit compositions with diverse functional characteristics (1). The KCNQ1 K^+ channel α subunit is widely distributed in both excitable and non-excitable cells of vertebrates, and is unique among the S4 gene superfamily in that it forms either voltage-activated or constitutively active K^+-selective channels depending on its specific KCNE family β subunit partner (2). *KCNQ1* and *KCNE* gene disruption are linked to multiple pathologies, often with an unclear molecular etiology. A sequence variant in exon 2 of human *KCNE2*, a gene associated with the cardiac arrhythmia long QT syndrome (LQTS) (3), has been implicated in a human cardiocerebral phenotype comprising both neonatal seizures and LQTS (4). In addition, duplication of a 200 kb region containing *KCNE1* and *KCNE2* has been detected in 16 individuals with schizophrenia but not in 7 control subjects (5). These findings suggested potential cerebral functions for KCNE2 (a protein we originally named MinK-related peptide 1). KCNE2 protein abundance is relatively low in neuronal tissue, but it is high in the fourth and lateral ventricles, in the apical membrane of the choroid plexus epithelium, where we have also detected KCNQ1 (6). KCNQ1, which is typically found in complexes with either KCNE2 or KCNE3, each of which render KCNQ1 constitutively active, is important in various non-excitable polarized epithelial cell types. In several of these epithelial tissues, KCNQ1-containing channels appear to be prerequisite for the function of ion transporters or symporters, although the molecular mechanisms for this necessity are unclear (6–8). Here, while investigating the basis for the increase in neural excitability in *Kcne2*$^{-/-}$ mice, we discovered an ion channel-transporter signaling complex, the perturbation of which caused the CNS metabolite imbalance underlying increased excitability.

Results

Kcne2 gene deletion in mice increased pentylenetetrazole-induced seizure susceptibility and mortality (Fig. 1B). Because intronic variants in human *KCNE2* have also been associated with psychiatric disorders (5), we assessed the behavior of *Kcne2*$^{-/-}$ mice. *Kcne2* deletion reduced the amount of time spent immobile in the tail suspension test by ~40% (which measures depression-like behavior and/or stress responsiveness) indicative of heightened stress response and/or reduced despair in *Kcne2*$^{-/-}$ mice compared to their *Kcne2*$^{+/+}$ mice littermates (9, 10) (Fig. 1C). *Kcne2* deletion did not affect motor function or balance (Fig. S1A) or overall activity (total locomotion or rearing) (Fig. S1 B,C).

KCNE2 abundance in the CNS is highest in the choroid plexus epithelium (6), which is the major site of CSF production and secretion, but *Kcne2* deletion does not substantially perturb CSF K^+ concentration or pH (6). We therefore adopted an untargeted CSF metabolomics approach to discover potentially pathologic CSF milieu disturbances. Unsupervised principle component analysis (PCA) of liquid chromatography/mass spectrometry (LC/MS) findings demonstrated a robust and consistent difference between CSF from *Kcne2*$^{-/-}$ compared to *Kcne2*$^{+/+}$ mice (Fig. 1D). We identified the features that contributed most significantly to this inter-genotype difference in CSF metabolites based on loading plot values for the PCA analysis (Fig. 1E). The single greatest contributor to the observed PCA difference was tentatively identified as *myo*-inositol which was confirmed by a LC retention time and MS/MS fragmentation pattern indistinguishable with those of a pure *myo*-inositol standard. Extracted ion counts verified that the 30% reduction in the concentration of *myo*-inositol in *Kcne2*$^{-/-}$ CSF was significant (Fig. 1F).

This finding was notable for two reasons. First, it was specific because *myo*-inositol was the only metabolite in the CSF whose abundance depended on *Kcne2*. Second, *myo*-inositol is actively transported into the CSF from the blood primarily through the choroid plexus epithelium to attain a CSF:blood *myo*-inositol ratio of >5:1 (11). In accord with perturbation of the concentration of *myo*-inositol, which is an important osmolyte, *Kcne2* deletion altered choroid plexus epithelial cell shape and volume (Fig. S2). Strikingly, acute CSF supplementation of *myo*-inositol dose-dependently reversed behavioral abnormalities and reduced pentylenetetrazole-induced seizure susceptibility in *Kcne2*$^{-/-}$ but not *Kcne2*$^{+/+}$ mice (Fig. 1G–J), suggesting that these defects were linked to the reduction in CSF *myo*-inositol in *Kcne2*$^{-/-}$ mice. The serum concentration of *myo*-inositol in *Kcne2*$^{-/-}$ mice was not significantly different from that of *Kcne2*$^{+/+}$ mice (Fig. 1H), a finding that was independently confirmed with a different MS system (Fig. 2A), suggesting a local perturbation of *myo*-inositol active transport at the level of the choroid plexus rather than a systemic defect in *myo*-inositol homeostasis. Furthermore, *Kcne2* deletion did not alter total SMIT1 protein abundance in mouse choroid plexus epithelium or kidney (Fig. 2B).

Despite the controversy surrounding the role of variations in the CSF concentration of *myo*-inositol in psychiatric disease (11, 12), our data suggest that the perturbation in CSF *myo*-inositol content is associated with a pathological CNS excitability in the *Kcne2*-deficient mouse. *myo*-inositol supplementation did not affect *Kcne2*$^{+/+}$ mice, but normalized two phenotypes indicative of ‘increased excitability’ in *Kcne2*$^{-/-}$ mice: increased seizure

activity, and increased mobility in the tail suspension test, which probably reflects an increased responsiveness to stress (10) and if validated by antidepressants could potentially be further interpreted as decreased depression-like behavior (9).

Na^+-coupled *myo*-inositol transporter SMIT1 (which is encoded by *SLC5A3*) mRNA has been previously detected in the choroid plexus epithelium (13). We visualized SMIT1 protein in mouse choroid plexus epithelium, employing tissue from *Slc5a3*$^{-/-}$ mice as a negative control for immunofluorescence detection. SMIT1 protein was detectable in both the apical and basolateral membranes of the choroid plexus epithelium (Fig. 2C and Fig. S3A,B). *Kcne2* deletion did not alter the membrane abundance of SMIT1. In some sections SMIT1 apical membrane abundance was less prominent (Fig. 2D), possibly reflecting regional variability in or dynamic control of SMIT1 localization, or simply variable antigen accessibility. The presence of SMIT1 on both basolateral and apical membranes of the choroid plexus epithelium suggests it could play a role both in myo-inositol uptake from the blood, and also in removing excess myo-inositol from the CSF.

We detected KCNQ1 and KCNE2 only on the apical membrane of the choroid plexus epithelium (Fig. 2E,F) as previously described (6). We also detected choroid plexus epithelial KCNQ1-KCNE2 and Kv1.3-KCNE2 protein complexes (Fig. 2G) as expected from our prior functional studies (6). In addition, we found that KCNE2 and KCNQ1 co-assembled with SMIT1 in the choroid plexus epithelium (Fig. 2G,H). KCNQ1 and SMIT1 colocalized in choroid plexus apical membrane (Fig. S3C).

SMIT1-KCNQ1 co-assembly was confirmed in heterologous co-expression studies (Fig. 3A). When co-expressed in *Xenopus laevis* oocytes, SMIT1 doubled KCNQ1 outward K^+ current (Fig. 3B,C) without affecting voltage dependence of activation (Fig. S4A). The current doubling was independent of external *myo*-inositol (Fig. 3D) or Na^+ (Fig. S4B). SMIT1 similarly doubled KCNQ1-KCNE2 channel current density in a *myo*-inositol-independent manner (Fig. 3E,F). In contrast, SMIT1 neither co-immunoprecipitated with KCNQ4 (which is closely related to KCNQ1) (Fig. 3G) nor altered KCNQ4 current density, which was also unaffected by SMIT2 (Fig. 3H).

Reciprocally, co-expression of KCNQ1, but not of KCNQ4, doubled steady-state *myo*-[$^{2\text{-}3}$H(N)] inositol uptake by SMIT1, although these channels have similar voltage-dependent activation properties (Fig. 4A). However, KCNQ1-KCNE2 (but not KCNE2 alone) inhibited SMIT1 steady-state *myo*-[$^{2\text{-}3}$H(N)] inositol uptake by ~70%, an effect that was not overcome by doubling the amount of SMIT1 cRNA injected while maintaining KCNQ1-KCNE2 cRNA constant (Fig. 4B). This was inconsistent with an exclusively electrochemical gradient-based explanation for KCNQ1 effects on SMIT1 given that KCNE2 converts KCNQ1 to a constitutively active K^+ channel and therefore drives the membrane potential toward the equilibrium potential for K+ (E_K). This membrane hyperpolarization (compared to that of cells expressing the homomeric, voltage-dependent KCNQ1 channel) increases the driving force (under physiological conditions) for inward Na^+ movement such as occurs during electrogenic *myo*-inositol active transport, and would therefore be predicted to increase, rather than decrease, *myo*-inositol uptake by SMIT1 (14). Similarly, co-expression of a form of KCNQ1 harboring a voltage sensor point mutation

(R231A) that confers constitutive channel activation (2) also strongly inhibited SMIT1 activity (~80%; Fig. 4A). When wild-type KCNQ1 was co-expressed, SMIT1 activity was sensitive to KCNQ inhibitor XE991, a sensitivity that was attenuated by the R231A mutation (Fig. 4C). SMIT1 *myo*-[$^{2\text{-}3}$H(N)] inositol uptake was still Na^+-dependent when KCNQ1 was coexpressed (Fig. 4D).

In contrast to SMIT1, SMIT2 decreased KCNQ1 current by 60% at +60 mV (without affecting KCNQ4, Fig. 3H). Like SMIT1, the structurally related Na^+-dependent glucose transporter SGLT1 augmented KCNQ1 current (by 40%); in contrast, the structurally related Na^+-dependent monocarboxylate transporter (SMCT) did not alter KCNQ1-current density (Fig. 5A,B). Similar to SMIT1, the effects of SMIT2 and SGLT1 on KCNQ1 did not involve altered voltage dependence and did not require external *myo*-inositol nor Na^+ (Fig. S4A,C–F). SMIT2 also inhibited KCNQ1-KCNE2 current (by ~50% at +60 mV; Fig. S5A,B). The effects of the transporters on channel activity were consistent over multiple oocyte batches (Fig. 5C).

Macroscopic (whole-oocyte) SMIT2 *myo*-[$^{2\text{-}3}$H(N)] inositol uptake was suppressed by the R231A-KCNQ1 mutant but not by wild-type KCNQ1 (whether KCNE2 was coexpressed or not) (Fig. 5D). Wild-type KCNQ1 (whether KCNE2 was coexpressed or not) rendered SMIT2 susceptible to inhibition by the KCNQ1-specific blocker (−)-[3R,4S]-Chromanol 293B (Fig. 5E) without altering sensitivity to phlorizin addition or Na^+ removal (Fig. S5C,D).

Discussion

Our findings demonstrate the existence of co-regulatory ion channel-transporter signaling complexes in biological systems. Although it is possible these complexes form to provide proximity such that K^+ efflux through the channel maintains a local electrical gradient facilitating electrogenic Na^+ influx, the observed sensitivity of transporter activity to KCNQ1 voltage sensor and/or pore status, with functional effects counter to predicted driving force effects, suggest intimate functional and physical coupling.

Myo-inositol, an osmolyte involved in cell volume regulation, is also a precursor for cell signaling substrates including phosphatidylinositol and phosphatidylinositolphosphate lipids such as phosphatidylinositol 4,5-bisphosphate (PIP_2) (15). Because KCNQ1 is both PIP_2- and cell volume-sensitive (16, 17), direct KCNQ1-SMIT1/2 interaction provides multiple potential feedback mechanisms to control cellular signaling and homeostasis. Notably, *Kcne2* deletion suppresses HCN channel function (I_h) in mouse thalamocortical circuits, increasing intrinsic excitability-enhanced burst firing in response to 4-aminopyridine, despite the relative paucity of neuronal KCNE2 expression (18). Given that HCN activity is augmented by PIP_2 *in vivo* and *in vitro* (19), it is tempting to speculate that the increased seizure susceptibility of *Kcne2*$^{-/-}$ mice arises from altered PIP_2 homeostasis because of a perturbation in *myo*-inositol transport. However, it may not be as simple as this. Prenatal *myo*-inositol treatment through maternal drinking water rescues *Slc5a3*$^{-/-}$ mice from congenital central apnea, without restoring fetal brain *myo*-inositol concentrations. Furthermore, there does not appear to be a phosphatidylinositol deficiency in *Slc5a3*$^{-/-}$

mice, and the mechanisms underlying both pathology and therapy in *Slc5a3*$^{-/-}$ mice are still not well understood (20).

Mechanisms underlying the blood:CSF *myo*-inositol gradient and its disruption by *Kcne2* deletion also remain incompletely resolved. However, based on our data we suggest that choroid plexus *myo*-inositol uptake from the blood through basolateral SMIT1 is unaffected, whereas removal of KCNE2 from apical SMIT1-KCNQ1-KCNE2 complexes increases *myo*-inositol reuptake from the CSF into the choroid plexus epithelium (consistent with data in Fig. 4B), reducing CSF *myo*-inositol content. The role of KCNQ1-KCNE2 in CSF *myo*-inositol homeostasis may impact multiple CNS disorders in which CSF *myo*-inositol homeostasis has been implicated (21–23), including the cognitive deficits associated with Down's syndrome (24), which is of particular interest because *KCNE2* is located on human chromosome 21.

KCNQ1-KCNE2 is also required *in vivo* for normal activity of the sodium iodide symporter (NIS) and the gastric H^+K^+ATPase (7, 8, 25). Furthermore, *KCNQ1* gene variants are linked to diabetes (26, 27) yet the underlying mechanisms have been elusive. It remains to be determined if any of these processes necessitate KCNQ1-transporter complexes, whether KCNQ1 interacts with transporters in excitable cells such as cardiac myocytes, and the extent to which other ion channels and transporters participate in co-regulatory complexes.

Materials and Methods

Animal use

We generated and genotyped the *Kcne2*$^{-/-}$ mouse line as previously described (24) and housed and used 4-month-old mice according to the US National Institutes of Health *Guide for the Care and Use of Laboratory Animals.* Animal procedures were approved by the Animal Care and Use Committee at Weill Medical College of Cornell University. The *Slc5a3*$^{-/-}$ mouse line was generated as previously described (20, 28). Animal procedures were approved by the Institutional Animal Care and Use Committee at Boston Children's Hospital. All mice used in this study were generated from heterozygous crosses.

Data presentation and statistics

Continuous data are expressed as means ± standard error of the mean (SEM) of *n* independent measurements. Dichotomous data are presented as percent. Statistical comparisons were generally by 1 test or one-way analysis of variance (ANOVA) followed by or 2-tailed, unpaired Student's *t* Bonferroni's *post hoc* test, with two exceptions: seizure incidence percentages were compared using two-sided z-statistic test for proportions. In all cases, statistical significance was assumed with $P < 0.05$.

Seizure susceptibility measured by pentylenetetrazole test

Seizure susceptibility measurements were performed as previously described (29). Briefly, pentylenetetrazole (Sigma-Aldrich) was dissolved in PBS and injected intraperitoneally to a concentration of 40–80 mg/kg bodyweight. Seizure events were observed over a period of 20 min. Mice were scored by an investigator blinded to genotype, for the sequence of four

seizure behaviors produced: myoclonic jerks, clonic convulsions, tonic phase and death. Timing of the seizures and their duration after pentylenetetrazole injection was recorded. Myoclonus was defined as a single movement of the mouse that involved a downward motion of the head, combined with a single jerk of the body, and a brief upward extension of the tail. Clonus was usually the second seizure behavior to occur chronologically after pentylenetetrazole injection and was defined as rapidly repetitive, often violent jerks of the mouse that involved the entire body, typically ending with the mouse falling to one side. The tonic stage of the seizure, when reached, was defined as a slow hind limb extension. Tonic stage was in some cases followed by death. Where appropriate, intraperitoneal injection of *myo*-inositol in vehicle (saline), or of vehicle alone, was performed by a non-scorer 30 min prior to intraperitoneal injection of pentylenetetrazole.

Behavioral tests

The tail suspension test (TST) was performed according to standard procedure (9), with the scorers blinded to genotype and content of injections. Where appropriate, intraperitoneal injection of *myo*-inositol or (−)-[3R,4S]-Chromanol 293B in vehicle (PBS), or of vehicle alone, was performed by a non-scorer 30 min prior to testing. Rotarod and open field tests were performed as previously described by M.T. and B.Z.(30); rotarod performance was timed manually, and open field test performance quantified digitally, both by a scorer blinded to genotype.

CSF Metabolomics/mass spectrometry (MS)

CSF was isolated from the cisterna magna of 3–6 month old *Kcne2*$^{+/+}$ and *Kcne2*$^{-/-}$ mice using a modification of a previously described technique (31). Briefly, mice were initially anesthetized with 1% isoflurane in 100% oxygen in a Plexiglas chamber and then placed in a small animal stereotaxic apparatus (model 900, David Kopf Instruments, Tujunga, CA) fitted with a mouse anesthesia mask (David Kopf Instruments) with ear bars to minimize movement of the head. With the head locked in place, the body of the mouse was allowed to drop, allowing access to the neck region. The neck was shaved, and an incision made using a sterile scalpel (no. 10 blade) and the muscles of the neck separated by blunt dissection to reveal the cisterna magna. Glass borosilicate capillary tubes (B100-78-10, Sutter Instrument, Novato, CA), pulled on a vertical micropipette puller (PP-830, Narishige, Japan) to generate a tapered tip with an inner diameter of roughly 0.6 mm were then used to penetrate the cisterna magna and CSF was drawn into the capillary tubes. A 1 ml syringe with polyethylene tubing attached to the end (to allow tight connection with the capillary tube) was then used to remove the CSF from the capillary tube. CSF samples were then placed on dry ice and transferred to −80° C until analysis. Mice were then killed by CO_2 asphyxiation. For MS data acquisition, CSF samples were extracted 1:20 in 70% acetonitrile (ACN) containing 0.2% acetic acid, vortexed, and centrifuged at 15,000 RPM for 10 min to remove cell debris. Supernatants were transferred to 250 μL conical polypropylene vials, capped and loaded into the liquid chromatography (LC) autosampler for analysis. Samples (2 μL) were analyzed using an LC-MS system and platform for untargeted metabolite profiling. A 1200 Series LC system (Agilent Technologies, Santa Clara, CA) with a 2.1 × 150 mm Cogent Diamond Hydride™ column (3.5 μm particle size, Microsolv Technology Corp, Eatontown, NJ) was utilized for chromatographic separation. MS analysis on post-column flow used

Agilent Series 6230 Accurate Mass time-of-flight (TOF) mass spectrometer, equipped with dual spray electrospray ionization (ESI) source, operating in positive ion mode.

LC parameters for ANP separation were as follows: 2 μl injection volume, 25°C column temperature, and a 0.4 ml/min mobile phase flow rate. The mobile phase consisted of 0.2% acetic acid in ddH_2O (solvent A) and 0.2% acetic acid in acetonitrile (solvent B) with gradient steps as follows: 0–2 min, 85% B; 2–3 min, to 80% B; 3–5 min, 80% B; 5–6 min, to 75% B; 6–7 min, 75% B, 7–8 min, to 70% B; 8–9 min, 70% B; 9–10 min, to 50% B; 10–11 min, 50% B, 11.0–11.1 min, 20% B; 11.1–14 min, 20% B; 14–14.1 min, 5% B; 14.1–24 min, 5% B; 24–24.1 min, 85% B and 24–34 min, 85% B. A separate isocratic pump delivered reference mass solution (ions m/z 121.0509 and 922.0093) for continuous mass calibration during sample analysis. Spectra were acquired in 2 GHz (extended dynamic range) mode with 1.71 spectra/sec sampled over a mass/charge (m/z) range of 50–1000 Daltons. The TOF capillary voltage was set at 4000 V, the fragmenter at 175 V, the nebulizer pressure was 35 psi, and 250°C nitrogen drying gas was delivered at a flow rate of 12 l/min.

MS Data Analysis

Raw data files were processed using Agilent MassHunter Qualitative Analysis Software (B346). Molecular feature extraction (MFE) generates information in features (compounds) that are stored in files for downstream comparative data analysis by MassProfiler Professional Software (Agilent). The analytical approach employs an algorithm for data alignment across multiple groups and treats all imported files as a single dataset. Following feature alignment and quality control, the unsupervised pattern recognition algorithm principal component analysis (PCA) was chosen to examine data sets for similarly changing features, expected and unexpected clusters, and the presence of outlying samples. Compounds determined to be differentially expressed based on statistical criteria and PCA results were assigned tentative formulae by utilizing a molecular formula generator (MFG) algorithm in Massprofiler Professional or MassHunter Qualitative Analysis. The MFG algorithm assigned molecular formula based on an optimized goodness-of-fit, considering accurate measurements of mass defect, natural isotopic abundance rations, and spacing between isotope peaks. A putative compound ID was tentatively assigned based on the MFG score and confirmed by comparison with retention times and MS/MS fragmentation of pure chemical standards.

Confirmatory quantification of myo-inositol in serum

myo-inositol was purchased from Sigma-Aldrich. LC-MS grade of acetonitrile, methanol and sonic dismembrator model 100 were purchased from Fisher Scientific. The internal standard, [$^2H_6$]-myo-inositol(MID6), was purchased from Cambridge Isotope Laboratories, Inc.(MA, USA).

Mouse serum was obtained by cardiac puncture in anesthetized mice for the collection of whole blood. The serum was deproteinized by addition of 4 volumes of 20 μmol/L of MID6 prepared in acetonitrile/water 80:20(v/v) to 1 volume of serum samples. The samples were vortexed thoroughly and centrifuged at 14000 rpm for 15 min. The supernatant was removed

and diluted 10 fold with MQ water. Samples were vortexed and centrifuged again prior to LC-MS/MS analysis. All serum samples were prepared in duplicates.

For calibration standards, stock solutions of *myo*-inositol were prepared in MQ water at a final concentration of 10 mM. The calibration standard concentrations were 500, 125, 31.25, 7.81 and 1.95 μmol/L of *myo*-inositol, also prepared in MQ water. 20 μl of each standard was mixed with 80 μl of 20 μmol/L of MID6 and 900 μl of MQ water.

A Shimadzu Prominence HPLC system was used to separate samples and standards with a SUPELCOGEL Pb column (300×7.8 mm;5μm; Supelco). The injection volume was 20ul and column temperature was set at 85°C. The HPLC protocol consisted of an isocratic gradient of 100% MQ water over a 45 min period. The flow rate was 0.5ml/min and was diverted to waste from 0–16min and 28–45min. The HPLC was coupled to a triple quadrupole tandem mass spectrometer equipped with an electrospray ionization source (AB Sciex QTRAP5500). It was operated in negative mode using the following settings: curtain gas 50, ion spray voltage −4500V, dissolvation temperature 550 degrees Celsius, gas1 40, gas2 40 and declustering potential and collision energy −60, −23 for inositol transition 179.0/87.0 and −55, −15 for MID6 transition 185.1/167.0 respectively. LC-MS/MS peak areas were integrated using Analyst 4.0 software. Further data analysis was performed on Excel (Microsoft).

Electron microscopy

For electron microscopy, choroid plexus tissue from the fourth ventricle of *Kcne2*$^{+/+}$ and *Kcne2*$^{-/-}$ mice (2/gender/genotype) was washed, fixed, stained, dehydrated and then infiltrated and embedded in Spurr's resin. Sections were cut, contrasted with lead citrate, and viewed on a JSM 100 CX-II electron microscope (JEOL USA Inc., Peabody, MA) operated at 80 kV. Images were recorded on Kodak 4489 Electron Image film and then digitized on an Epson Expression 1600 Pro scanner at 900 dpi.

Immunofluorescence detection

Tissue samples from *Kcne2*$^{+/+}$ and *Kcne2*$^{-/-}$ mice were fixed in 4% paraformaldehyde solution (Electron Microscopy Sciences, Hatfield, PA, USA), followed by incubation in 30% sucrose overnight at 4°C. Embedding was performed in an optimal cutting temperature (OCT) compound (Tissue-Tek, Torrance, CA, USA), and embedded samples were stored at −80°C. Frozen samples were cut into 10 μm thick sections (Cryomicrotome CM 1850, Leica Microsystems, Bannockburn, IL, USA). Immunofluorescence detection of Kcnq1, Smit1 and Nkcc1 was performed by either of two methods. First, using a Discovery XT processor (Ventana Medical Systems), goat polyclonal anti-KCNQ1 (pan-species) primary antibody (Santa Cruz Biotechnology #SC-10646) was used at 1mg/ml; mouse monoclonal anti-NKCC1 (Santa Cruz Biotech) at 1:500 dilution; rabbit polyclonal anti-SMIT1 (1:500, Santa Cruz Biotechnology) at 1:500 dilution. Preceding the primary antibody incubation, tissue sections were blocked for 30 minutes in 10% normal goat, rabbit or mouse serum, 2% BSA in PBS, followed by 8 minutes Avidin/Biotin block. The primary antibody incubation (3 hours) was followed by incubation with biotinylated anti-rabbit, mouse or goat IgG as appropriate (ANC kit from Vector labs). The secondary detection was performed with

Streptavidin-HRP D (Ventana Medical Systems), followed by incubation with Tyramide-Alexa Fluor secondary antibodies (Invitrogen). Alternatively, for images in Fig. 2C,D and Fig. S3, immunofluorescence detection was performed manually, with the experimenter blinded to the mouse genotype, after fixing/permeabilizing sections in ice-cold acetone for 10 minutes. Biotinylation was not employed for this approach; other experimental details were similar. Immunostained slides were viewed with an Olympus BX51 microscope and pictures were acquired using CellSens software (Olympus).

Xenopus laevis oocyte preparation

cRNA transcripts encoding human KCNE2, KCNQ1, R231A-KCNQ1 (2), KCNQ4, SMIT1, SMIT2, SGLT1 and SMCT were produced from linearized cDNA templates using the T3 or T7 mMessage mMachine kit (Ambion, Austin, TX). SMIT1 cDNA was purchased from Origene (Rockville, MD); SMIT2 and SGLT1 clones were a kind gift from Dr. Michael J. Coady and Dr. Jean-Yves Lapointe (GÉPROM, Université de Montréal); SMCT cDNA was a kind gift from Dr. Nancy Carrasco (Yale University). Channel subunit and transporter cRNA was quantified by spectrophotometry and size integrity verified by gel electrophoresis. Defolliculated stage V and VI *Xenopus laevis* oocytes (Ecocyte Bioscience, Austin, TX) were injected with one or more of the cRNAs above (KCNQ1, 10 ng; KCNE2, 4 ng/oocyte; transporters, 5–25 ng/oocyte as described in text). Oocytes were incubated at 16 °C in ND96 solution containing penicillin and streptomycin with daily washing, for 4–5 days before functional or biochemical assays.

Two-electrode voltage clamp (TEVC) and myo-[$^{2\text{-}3}$H(N)]-inositol flux assays

TEVC recordings were performed at room temperature using an OC-725C amplifier (Warner Instruments, Hamden, CT) and pClamp8 software (Molecular Devices, Sunnyvale, CA), 4–5 days after cRNA injection. Oocytes were bathed in a small-volume oocyte bath (Warner) and viewed with a dissection microscope. Bath solution was (in mM): 96 NaCl, 4 KCl, 1 $MgCl_2$, 1 $CaCl_2$, 10 HEPES (pH 7.6) (4K^+/96Na^+ solution) with/without Na^+ replacement by NMDG, and/or addition of phlorizin (500 μM) and/or *myo*-inositol (1 mM); bath chemicals were from Sigma Aldrich unless otherwise indicated. TEVC pipettes were of 8 MΩ resistance when filled with 3 M KCl. Currents were recorded with a Voltage protocol consisting of 3 s pulses between −120 mV and 60 mV at 20 mV intervals each followed by a 1 s tail pulse to −30 mV, from a holding potential of −80 mV.

TEVC data analysis was performed with pClamp8, Excel (Microsoft) and Origin 6.1 (OriginLab Corp., Northampton, MA). Values are stated as mean ± SEM. Normalized tail current was plotted versus prepulse voltage and fitted with a single Boltzmann function according to:

$$g=(A_1-A_2)/\{1+\exp[(V_{1/2}-V)/V_s]\}+A_2,$$

where g is the normalized tail conductance, A_1 is the initial value at $-\infty$, A_2 is the final value at $+\infty$, $V_{1/2}$ is the half-maximal voltage of activation and V_s the slope factor. KCNQ1 current activation curves were fitted with a standard (zero-shift) double exponential function with Chebyshev 4-point smoothing filter. Radiolabeled *myo*-inositol uptake assays using

myo-[$^{2\text{-}3}$H(N)] inositol (American Radiolabeled Chemicals, Inc, Saint Louis, MO, USA) were performed 5 days after oocyte cRNA injection. For each condition/expression group, 6–12 oocytes were placed in a round-bottomed, 10 ml culture tube, washed and resuspended in ND96 or NMDG-substituted ND96 (200 μl/tube) containing *myo*-[$^{2\text{-}3}$H(N)] inositol (3 μCi/ml) with/without phlorizin (Sigma) (500 μM), XE991 (Sigma) (10 μM) or C293B (Tocris) (20 μM). After 30 minutes at room temperature, oocytes were washed 2–3 times in 3 ml ND96 or NMDG-substituted ND96 containing 1 mM cold *myo*-inositol (Sigma) followed by 1–2 washes in 3 ml ND96. Oocytes were next individually placed in wells of a 96-well plate, lysed in 100 μl 2% SDS in ND96, then each lysed oocyte was transferred to a scintillation vial (1 oocyte/vial) containing Ready Protein Plus scintillation fluid (Beckmann Coulter, Fullerton, CA) (6 ml). Vials were capped, shaken vigorously, then allowed to sit at room temperature for at least 30 minutes before scintillation counting in a Beckmann Coulter 6500. Each experiment was performed on several batches of oocytes from different deliveries as described in the figure legends; results presented are either raw data from a single representative batch, or in some cases pooled data from 2 or more batches normalized to the mean value of uptake of the intra-batch control group (either transporter alone, or in the absence of inhibitor).

Protein biochemistry

For choroid plexus epithelial studies, adult *Kcne2*$^{+/+}$ and *Kcne2*$^{-/-}$ mice were killed by CO_2 asphyxiation, and the choroid plexus removed from the fourth ventricle of the brain. Tissue samples were then snap-frozen in liquid N_2 for use in western blot analysis. Whole choroid plexus cell lysates were isolated[3](32), resolved using SDS-PAGE and transferred to PVDF membranes for western blot analysis using standard techniques and equipment (Bio-Rad). Kidney tissue was similarly harvested and analyzed. PVDF membranes were incubated for 3 h at room temperature in 5% milk with primary antibodies, diluted as follows: rabbit polyclonal anti-KCNE2 (in-house) 1:1000; goat polyclonal anti-KCNQ1 (Santa Cruz Biotech) 1:1000; GAPDH (Bio Rad) 1:100. For secondary detection, horseradish peroxidase-conjugated species-appropriate anti-IgG antibodies (1:10.000, Bio-Rad) were used. Signals were detected with ECL-Plus chemiluminescence (Amersham Bioscience) and analyzed with a Gbox system using Gbox software (Syngene).

For *X. laevis* oocyte biochemistry, membrane fractions were prepared from oocytes injected with the appropriate cRNAs (see next section) as follows: 5–10 oocytes per group were homogenized in 1 ml lysis buffer containing: 0.3 M sucrose, 10 mM sodium phosphate and 1 mM EDTA supplemented with protease inhibitor cocktail (Sigma). The homogenate was subjected to a low spin centrifugation (4000 rpm; 15 min; 4 °C) to remove yolk protein and cell debris. Membrane fractions were then pelleted at 40,000 × g for 10 min for co-immunoprecipitation and/or western blot analysis. Protein concentrations were determined using the BCA method (Pierce, Rockford, IL, USA). For western blots, up to 5 μg of total protein was mixed with sample buffer and applied on 4–12% Bis-Tris SDS-PAGE gels (Invitrogen). Following electrophoresis, proteins were transferred onto nitrocellulose membranes (VWR). Membranes were incubated with goat anti-KCNQ1 polyclonal IgG (1:500, Santa Cruz Biotechnology), rabbit anti-SMIT1 (1:500, Santa Cruz Biotechnology), rabbit anti-SMIT2 (1:1000, MBL international) or rabbit anti-KCNQ4 (1:500, Santa Cruz

Biotechnology). Horseradish peroxidase (HRP)-conjugated goat anti-rabbit or rabbit anti-goat IgG secondary antibody (Bio-Rad) was used for visualization with chemiluminescence ECL (Millipore). Signals were analyzed with a Gbox system using Gbox software (Syngene).

For co-immunoprecipitations, whole choroid plexus epithelial cell lysates or *X. laevis* oocyte crude membrane fractions were incubated with goat anti-KCNQ1 polyclonal IgG (1:500, Santa Cruz Biotechnology), mouse monoclonal anti-Kv1.3 (1:500, NeuroMabs), mouse monoclonal anti-NKCC1 (1:500, Santa Cruz Biotechnology), rabbit anti-SMIT1 (1:500, Santa Cruz Biotechnology), or rabbit anti-KCNQ4 (1:500, Santa Cruz Biotechnology) for 4–12 h before precipitation with Protein A/G agarose beads (Pierce). The reactions were washed 3–4 times and samples were eluted prior to immunoblotting as described above.

For Chinese hamster ovary (CHO) cell biochemistry, CHO cells were transfected with cDNAs for KCNQ1 and/or SMIT1-DDK-MyC (Origene). Two days post-transfection, cells were lysed in buffer containing 150 mM NaCl, 1% IGEPAL, 50 mM Tris (pH 8.0), 0.1% SDS. Lysate were centrifuged at 3,000 rcf for 15 minutes at 4 °C and the pellets discarded. Lysates were normalized by total protein content (BCA Protein Assay kit, Pierce), mixed with NuPage LDS sample buffer (Life Technologies, Grand Island, NY) supplemented with 5% beta-mercaptoethanol, vortexed, heated at 37 °C for 10 minutes, then briefly centrifuged at 1,000 g for 3 minutes at room temperature. Lysate samples were then separated using a NuPage 4–12% bis-tris gel with NuPage antioxidant (Life Technologies) in MOPS running buffer. Following electrophoresis, proteins were transferred to either PVDF or nitrocellulose membranes in the following buffer: 0.037% LDS, 20% MeOH, 48mM Tris base, 39 mM glycine. Membranes were then blocked in a solution of PBST (PBS + 0.1% Tween-20) + 5% nonfat milk powder; incubated at room temperature for 1–2 hours. Membranes were incubated overnight at 4 °C in fresh PBST + 5% milk containing mouse monoclonal anti-DDK [1:2000] (Origene) or goat polyclonal KCNQ1 [1:1000] (Santa Cruz). After washing, membranes were incubated in PBST + 3% milk solution containing 1/5000-diluted HRP-conjugated secondary antibodies (Bio Rad) for 1 hour at room temperature. After further washing, membranes were incubated with Luminata Forte Western HRP substrate for 5 minutes and imaged with a Syngene G Box.

For CHO cell co-immunoprecipitations, 100 μg total protein from each lysate sample was diluted with lysis buffer to 500 μl total volume and then pre-cleared with protein A/G PLUS agarose beads (Santa Cruz). Following the pre-clear step, beads were pelleted by a 5 minute spin at 1,000 rcf, 4°C, and the supernatant transferred to a new tube. Immunoprecipitating antibodies, goat polyclonal anti-KCNQ1 (Santa Cruz) or mouse monoclonal anti-DDK (Origene), were added to a dilution of 1/100 for overnight incubation at 4°C. The following day, fresh protein A/G PLUS agarose beads were washed in lysis buffer, pelleted, and reconstituted in lysis buffer to a 50% suspension (v/v). 40 μl of this suspension was added to each of the IP tubes and mixed end-over-end for 4 hours at 4 °C. Beads were then pelleted, washed with lysis buffer (3×5 minutes), and then proteins eluted into NuPage LDS sample buffer for SDS-PAGE and western blotting as described above.

Acknowledgments

We sincerely thank N. Carrasco for the SMCT clone and M. Coady for the SMIT2 and SGLT1 clones. We are grateful to M. Anand for expert technical assistance, and N. Carrasco, I. Curtis, K. Duff, N. Harrison and C. Inturrisi for advice and other resources.

Funding: G.W.A. is grateful for support from the National Heart, Lung and Blood Institute, National Institutes of Health (R01 HL079275) and University of California, Irvine setup funds. S.S.G. is supported by a grant from the National Heart, Lung and Blood Institute, National Institutes of Health (R37 HL87062) and a grant from X (PO1 HD67244). G.T.B. is supported by a grant from the Manton Center for Orphan Disease Research

References and Notes

1. McCrossan ZA, Abbott GW. The MinK-related peptides. Neuropharmacology. 2004; 47:787–821. [PubMed: 15527815]
2. Panaghie G, Abbott GW. The role of S4 charges in voltage-dependent and voltage-independent KCNQ1 potassium channel complexes. J Gen Physiol. 2007; 129:121–33. [PubMed: 17227916]
3. Abbott GW, Sesti F, Splawski I, Buck ME, Lehmann MH, Timothy KW, Keating MT, Goldstein SA. MiRP1 forms IKr potassium channels with HERG and is associated with cardiac arrhythmia. Cell. 1999; 97:175–87. [PubMed: 10219239]
4. Heron SE, Hernandez M, Edwards C, Edkins E, Jansen FE, Scheffer IE, Berkovic SF, Mulley JC. Neonatal seizures and long QT syndrome: a cardiocerebral channelopathy? Epilepsia. 2010; 51:293–6. [PubMed: 19863579]
5. Tam GW, van de Lagemaat LN, Redon R, Strathdee KE, Croning MD, Malloy MP, Muir WJ, Pickard BS, Deary IJ, Blackwood DH, Carter NP, Grant SG. Confirmed rare copy number variants implicate novel genes in schizophrenia. Biochem Soc Trans. 2010; 38:445–51. [PubMed: 20298200]
6. Roepke TK V, Kanda A, Purtell K, King EC, Lerner DJ, Abbott GW. KCNE2 forms potassium channels with KCNA3 and KCNQ1 in the choroid plexus epithelium. FASEB J. 2011; 25:4264–73. [PubMed: 21859894]
7. Lee MP, Ravenel JD, Hu RJ, Lustig LR, Tomaselli G, Berger RD, Brandenburg SA, Litzi TJ, Bunton TE, Limb C, Francis H, Gorelikow M, Gu H, Washington K, Argani P, Goldenring JR, Coffey RJ, Feinberg AP. Targeted disruption of the Kvlqt1 gene causes deafness and gastric hyperplasia in mice. J Clin Invest. 2000; 106:1447–55. [PubMed: 11120752]
8. Roepke TK, King EC, Reyna-Neyra A, Paroder M, Purtell K, Koba W, Fine E, Lerner DJ, Carrasco N, Abbott GW. Kcne2 deletion uncovers its crucial role in thyroid hormone biosynthesis. Nat Med. 2009; 15:1186–94. [PubMed: 19767733]
9. Cryan JF, Mombereau C, Vassout A. The tail suspension test as a model for assessing antidepressant activity: review of pharmacological and genetic studies in mice. Neurosci Biobehav Rev. 2005; 29:571–625. [PubMed: 15890404]
10. Gleason G, Liu B, Bruening S, Zupan B, Auerbach A, Mark W, Oh JE, Gal-Toth J, Lee F, Toth M. The serotonin1A receptor gene as a genetic and prenatal maternal environmental factor in anxiety. Proc Natl Acad Sci U S A. 2010; 107:7592–7. [PubMed: 20368423]
11. Spector R, Johanson C. Micronutrient and urate transport in choroid plexus and kidney: implications for drug therapy. Pharm Res. 2006; 23:2515–24. [PubMed: 17048121]
12. Bersudsky Y, Shaldubina A, Agam G, Berry GT, Belmaker RH. Homozygote inositol transporter knockout mice show a lithium-like phenotype. Bipolar Disord. 2008; 10:453–9. [PubMed: 18452441]
13. Guo W, Shimada S, Tajiri H, Yamauchi A, Yamashita T, Okada S, Tohyama M. Developmental regulation of Na+/myo-inositol cotransporter gene expression. Brain Res Mol Brain Res. 1997; 51:91–6. [PubMed: 9427510]
14. Bourgeois F, Coady MJ, Lapointe JY. Determination of transport stoichiometry for two cation-coupled myo-inositol cotransporters: SMIT2 and HMIT. J Physiol. 2005; 563:333–43. [PubMed: 15613375]

15. Holub BJ. The nutritional significance, metabolism, and function of myo-inositol and phosphatidylinositol in health and disease. Adv Nutr Res. 1982; 4:107–41. [PubMed: 6278902]
16. Loussouarn G, Park KH, Bellocq C, Baro I, Charpentier F, Escande D. Phosphatidylinositol-4,5-bisphosphate, PIP2, controls KCNQ1/KCNE1 voltage-gated potassium channels: a functional homology between voltage-gated and inward rectifier K+ channels. EMBO J. 2003; 22:5412–21. [PubMed: 14532114]
17. Hammami S, Willumsen NJ, Olsen HL, Morera FJ, Latorre R, Klaerke DA. Cell volume and membrane stretch independently control K+ channel activity. J Physiol. 2009; 587:2225–31. [PubMed: 19289549]
18. Ying SW V, Kanda A, Hu Z, Purtell K, King EC, Abbott GW, Goldstein PA. Targeted Deletion of Kcne2 Impairs HCN Channel Function in Mouse Thalamocortical Circuits. PLoS One. 2012; 7:e42756. [PubMed: 22880098]
19. Pian P, Bucchi A, Robinson RB, Siegelbaum SA. Regulation of gating and rundown of HCN hyperpolarization-activated channels by exogenous and endogenous PIP2. J Gen Physiol. 2006; 128:593–604. [PubMed: 17074978]
20. Buccafusca R, Venditti CP, Kenyon LC, Johanson RA, Van Bockstaele E, Ren J, Pagliardini S, Minarcik J, Golden JA, Coady MJ, Greer JJ, Berry GT. Characterization of the null murine sodium/myo-inositol cotransporter 1 (Smit1 or Slc5a3) phenotype: myo-inositol rescue is independent of expression of its cognate mitochondrial ribosomal protein subunit 6 (Mrps6) gene and of phosphatidylinositol levels in neonatal brain. Mol Genet Metab. 2008; 95:81–95. [PubMed: 18675571]
21. Talisman IJ, Marzabadi CH. Carbohydrate-based drugs in the treatment of epilepsy, depression and other affective disorders. Curr Top Med Chem. 2008; 8:159–70. [PubMed: 18289085]
22. Firbank MJ, Harrison RM, O'Brien JT. A comprehensive review of proton magnetic resonance spectroscopy studies in dementia and Parkinson's disease. Dement Geriatr Cogn Disord. 2002; 14:64–76. [PubMed: 12145453]
23. Kofman O, Sherman WR, Katz V, Belmaker RH. Restoration of brain myo-inositol levels in rats increases latency to lithium-pilocarpine seizures. Psychopharmacology (Berl). 1993; 110:229–34. [PubMed: 7870890]
24. Huang W, Alexander GE, Daly EM, Shetty HU, Krasuski JS, Rapoport SI, Schapiro MB. High brain myo-inositol levels in the predementia phase of Alzheimer's disease in adults with Down's syndrome: a 1H MRS study. Am J Psychiatry. 1999; 156:1879–86. [PubMed: 10588400]
25. Roepke TK, Anantharam A, Kirchhoff P, Busque SM, Young JB, Geibel JP, Lerner DJ, Abbott GW. The KCNE2 potassium channel ancillary subunit is essential for gastric acid secretion. J Biol Chem. 2006; 281:23740–7. [PubMed: 16754665]
26. Unoki H, Takahashi A, Kawaguchi T, Hara K, Horikoshi M, Andersen G, Ng DP, Holmkvist J, Borch-Johnsen K, Jorgensen T, Sandbaek A, Lauritzen T, Hansen T, Nurbaya S, Tsunoda T, Kubo M, Babazono T, Hirose H, Hayashi M, Iwamoto Y, Kashiwagi A, Kaku K, Kawamori R, Tai ES, Pedersen O, Kamatani N, Kadowaki T, Kikkawa R, Nakamura Y, Maeda S. SNPs in KCNQ1 are associated with susceptibility to type 2 diabetes in East Asian and European populations. Nat Genet. 2008; 40:1098–102. [PubMed: 18711366]
27. Yasuda K, Miyake K, Horikawa Y, Hara K, Osawa H, Furuta H, Hirota Y, Mori H, Jonsson A, Sato Y, Yamagata K, Hinokio Y, Wang HY, Tanahashi T, Nakamura N, Oka Y, Iwasaki N, Iwamoto Y, Yamada Y, Seino Y, Maegawa H, Kashiwagi A, Takeda J, Maeda E, Shin HD, Cho YM, Park KS, Lee HK, Ng MC, Ma RC, So WY, Chan JC, Lyssenko V, Tuomi T, Nilsson P, Groop L, Kamatani N, Sekine A, Nakamura Y, Yamamoto K, Yoshida T, Tokunaga K, Itakura M, Makino H, Nanjo K, Kadowaki T, Kasuga M. Variants in KCNQ1 are associated with susceptibility to type 2 diabetes mellitus. Nat Genet. 2008; 40:1092–7. [PubMed: 18711367]
28. Berry GT, Wu S, Buccafusca R, Ren J, Gonzales LW, Ballard PL, Golden JA, Stevens MJ, Greer JJ. Loss of murine Na+/myo-inositol cotransporter leads to brain myo-inositol depletion and central apnea. J Biol Chem. 2003; 278:18297–302. [PubMed: 12582158]
29. Donovan GP, Harden C, Gal J, Ho L, Sibille E, Trifiletti R, Gudas LJ, Toth M. Sensitivity to jerky gene dosage underlies epileptic seizures in mice. J Neurosci. 1997; 17:4562–9. [PubMed: 9169517]

30. Zupan B, Toth M. Inactivation of the maternal fragile X gene results in sensitization of GABAB receptor function in the offspring. J Pharmacol Exp Ther. 2008; 327:820–6. [PubMed: 18812493]

31. Liu L, Duff K. A technique for serial collection of cerebrospinal fluid from the cisterna magna in mouse. J Vis Exp. 2008

32. Speake T, Freeman LJ, Brown PD. Expression of aquaporin 1 and aquaporin 4 water channels in rat choroid plexus. Biochim Biophys Acta. 2003; 1609:80–6. [PubMed: 12507761]

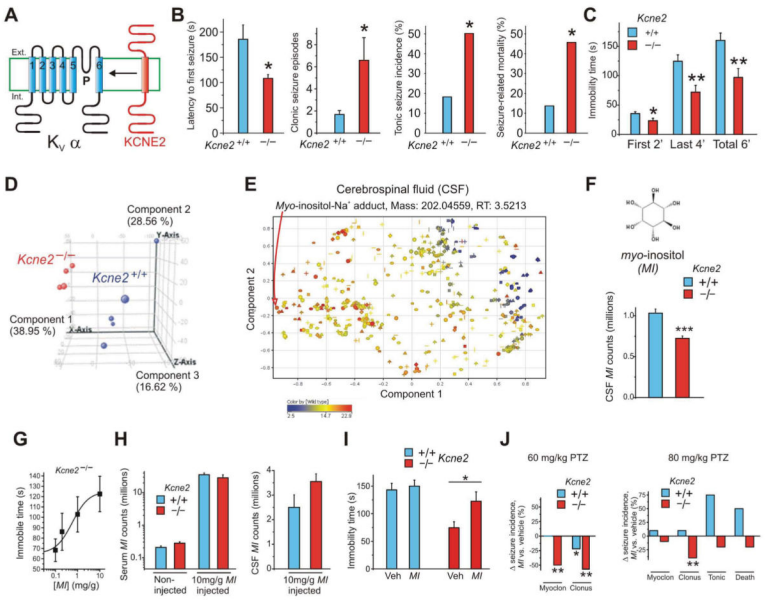

Figure 1. Global metabolite profiling reveals *Kcne2*$^{-/-}$ mice have depleted CSF *myo*-inositol, supplementation with which alleviates their neurological phenotypes

A. Transmembrane topology of Kv channel α subunit (blue) and KCNE2 (red).

B. Mean seizure activity during the first 20 minutes after injection of pentylenetetrazole in *Kcne2*$^{+/+}$ and *Kcne2*$^{-/-}$ mice; $n = 22$ mice per genotype. * $P<0.05$.

C. Mean immobility time, and immobile-to-mobile switches, during tail suspension test for *Kcne2*$^{+/+}$ and *Kcne2*$^{-/-}$ mice; $n = 15$ mice per genotype. * $P<0.05$; ** $P<0.01$.

D. Unsupervised principal component analysis (PCA) of CSF metabolites acquired by LC-MS in positive ion mode. Relative quantification of 586 features (defined by an accurate mass and retention time pair) was obtained in CSF from all samples in at least one genotype. Data points are a 3-D projection that summarizes the variance of all CSF features (metabolites) from an individual mouse as three principal components, quantified as coordinates on each of three graphical projections. Results show consistent clustering of CSF metabolites for both *Kcne2*$^{+/+}$ and *Kcne2*$^{-/-}$ mice. These genotypes were distinguished by principal component 1 (PC1; quantified on the X-axis), which accounted for >38% of total between-genotype variance.

E. Loading plot, depicting the relative contribution of individual features (metabolites) to the between-genotype variance observed for PC1 and PC2, as depicted in (D). The features that are most distant from the origin in PC1 are those that make the greatest contribution to distinguishing CSF in *Kcne2*$^{-/-}$ compared to *Kcne2*$^{+/+}$ mice. The single greatest contributor to PC1 variance (loading −0.948) (red arrow) was later identified as the Na^+ adduct of *myo*-inositol (RT, retention time).

F. Extracted ion chromatograms (EICs) for *myo*-inositol in CSF. Relative abundances for the Na^+ adduct of *myo*-inositol in CSF samples were calculated based on the area under EIC curves. The concentration of *myo*-inositol in CSF was significantly lower in *Kcne2*$^{-/-}$ compared to *Kcne2*$^{+/+}$ mice (30% decrease); $n = 4$–5 mice per genotype. ***P <0.002.

G. Dose-dependent effects of intraperitoneal injection of *myo*-inositol on the immobility of *Kcne2*$^{-/-}$ mice during the final four minutes of the tail suspension test; n = 9–20 mice per dose.

H. Serum (***left***) and CSF (***right***) concentrations of *myo*-inositol in non-injected and *myo*-inositol-injected mice. No significant genotype-dependent differences (P>0.05).

I. Comparison of effects of *myo*-inositol (n = 10–15 mice per group) on immobility time of *Kcne2*$^{+/+}$ and *Kcne2*$^{-/-}$ mice in the tail suspension test. *Significantly different from values obtained for non-injected and vehicle-injected *Kcne2*$^{-/-}$ mice only ($P < 0.05$).

J. Effects of *myo*-inositol on seizure incidence during the first 20 minutes following injection of pentylenetetrazole; n = 10 mice per group. Significant difference from same-genotype, vehicle-injected mice: *P < 0.05; **P < 0.01.

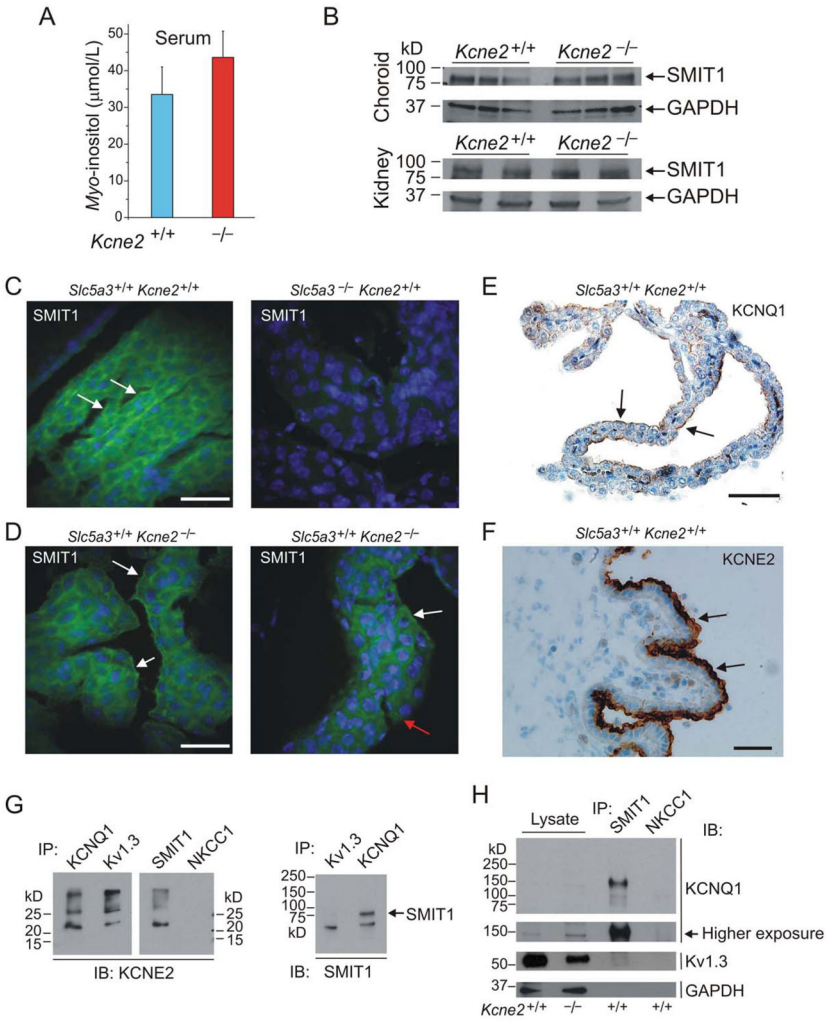

Figure 2. KCNE2 and KCNQ1 co-assemble with SMIT1 in mouse choroid plexus epithelium

A. Mean serum *myo*-inositol concentration of *Kcne2*$^{+/+}$ and *Kcne2*$^{-/-}$ mice (n = 5 mice/genotype).

B. Western blots of mouse *Kcne2*$^{+/+}$ and *Kcne2*$^{-/-}$ choroid plexus epithelium and kidney lysates showing no appreciable effect of *Kcne2* deletion on SMIT1 protein abundance, with GAPDH as a loading control (each lane using lysate from a different mouse).

C. Representative (of multiple sections from n = 2 mice per genotype) immunofluorescence images of adult *Slc5a3*$^{+/+}$ and *Slc5a3*$^{-/-}$ mouse choroid plexus epithelium. White arrows, apically localized SMIT1. Scale bar: 40 μm. Green, anti-SMIT1 antibody; blue, DAPI.

D. Representative (of multiple sections from n = 2 mice per genotype) immunofluorescence images of adult *Kcne2*$^{-/-}$ mouse choroid plexus epithelium showing regions of apical membrane regions with (white arrows) or without (red arrow) SMIT1 signal. Scale bar: 40 μm. Green, anti-SMIT1 antibody; blue, DAPI.

E. Immunohistochemistry of adult *Kcne2*$^{+/+}$ mouse choroid plexus epithelium, showing apical localization of KCNQ1 (arrows). Scale bar: 80 μm. Brown, anti-KCNQ1 antibody; representative of n = 3 mice.

F. Immunohistochemistry of adult *Kcne2*$^{+/+}$ mouse choroid plexus epithelium, showing apical localization of KCNE2 (arrows). Scale bar: 40 μm. Brown, anti-KCNE2 antibody; representative of $n = 3$ mice.

G. Western blots using immunoblotting (IB) antibodies as indicated, on adult *Kcne2*$^{+/+}$ mouse choroid plexus epithelium lysates and immunoprecipitates (IP) using IP antibodies as indicated. ***Left,*** KCNE2 forms complexes with each of KCNQ1, Kv1.3 and SMIT1, but not NKCC1. ***Right,*** SMIT1 (*arrow*) forms complexes with KCNQ1 but not Kv1.3. Representative of $n = 2$ experiments.

H. Western blots using immunoblotting (IB) antibodies as indicated, on adult *Kcne2*$^{+/+}$ and *Kcne2*$^{-/-}$ mouse choroid plexus epithelium lysates and immunoprecipitates (IP) using IP antibodies as indicated. KCNQ1 (but not Kv1.3 or GAPDH) forms complexes with SMIT1 (but not NKCC1). Representative of $n = 2$ experiments. *Arrow*, higher exposure of blot directly above, to show KCNQ1 bands in the lysate.

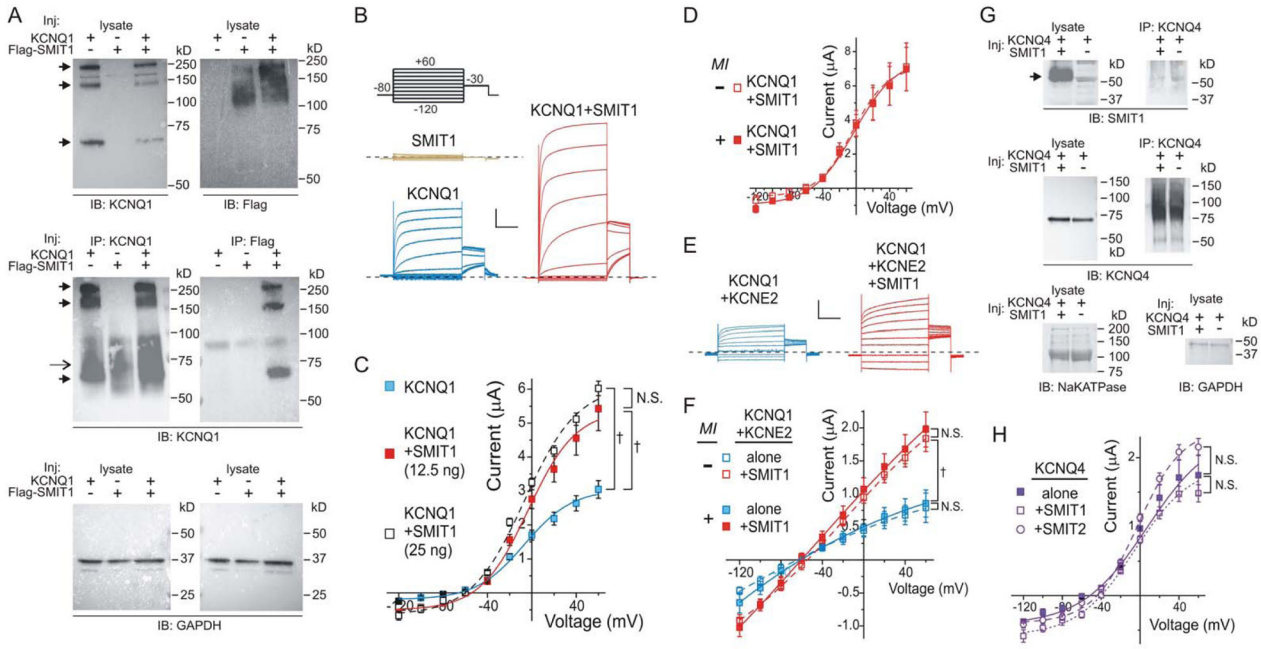

Figure 3. SMIT1 co-assembles with and augments activity of KCNQ1-KCNE2

A. Western blots using immunoblotting (IB) antibodies as indicated, on CHO cell lysates (***upper blots***) and immunoprecipitates (IP) (***middle blots***) using IP antibodies as indicated. Cells were transfected with KCNQ1 and/or Flag-tagged SMIT1 cDNA as indicated. Filled arrowheads indicate the characteristic monomer, dimer and tetramer banding pattern of heterologously expressed KCNQ1. Single arrow indicates precipitating antibody detected by secondary antibody. ***Lower blots:*** GAPDH loading controls for lysates used in gels above. Results representative of 2 independent experiments.

B. Exemplar current traces recorded in oocytes expressing SMIT1 and/or KCNQ1 using the standard voltage family protocol (inset). Scale bars: vertical, 1 μA; horizontal, 1 s. Zero current level indicated by dashed line.

C. Mean raw current-voltage relationships for oocytes co-injected with KCNQ1 cRNA with or without the amount of SMIT1 cRNA indicated; n = 21 (KCNQ1), 7 (SMIT1+KCNQ1, 12.5 ng), 11 (SMIT1+KCNQ1, 25 ng). † P<0.0005 at 60 mV. N.S., non-significant (P>0.05).

D. Mean raw macroscopic current-voltage relationships for oocytes in ND96 bath solution, with or without *myo*-inositol, co-injected with KCNQ1 cRNA and SMIT1 cRNA; n = 4–5 oocytes per group.

E. Exemplar current traces recorded in oocytes expressing SMIT1 and/or KCNQ1-KCNE2 using the standard voltage family protocol (panel B). Scale bars: vertical, 0.5 μA; horizontal, 1 s. Zero current level indicated by dashed line.

F. Mean raw current-voltage relationships for oocytes as in **E**, with or without *myo*-inositol in bath solution; n = 5–10 oocytes per group. †P<0.01 at 60 mV. N.S., non-significant (P>0.05).

G. ***Upper:*** western blots of membrane-fractionated lysate (*left*) and anti-KCNQ4 antibody immunoprecipitated (IP) fraction (*right*) of *X. laevis* oocytes injected (Inj) with cRNA encoding KCNQ4 and/or SMIT1 and immunoblotted (IB) with anti-SMIT1 antibody.

Arrow, the expected migration distance for SMIT1. Results representative of 2 independent experiments. ***Middle:*** as above but IB with anti-KCNQ4 antibody. ***Lower***, Na^+/K^+ATPase (left) and GAPDH (right) loading controls for lysates.

H. Mean raw current-voltage relationships for oocytes expressing SMIT1 or SMIT2 and/or KCNQ4 using the standard voltage family protocol (panel B); n = 9–12 oocytes per group. N.S., non-significant (P>0.05).

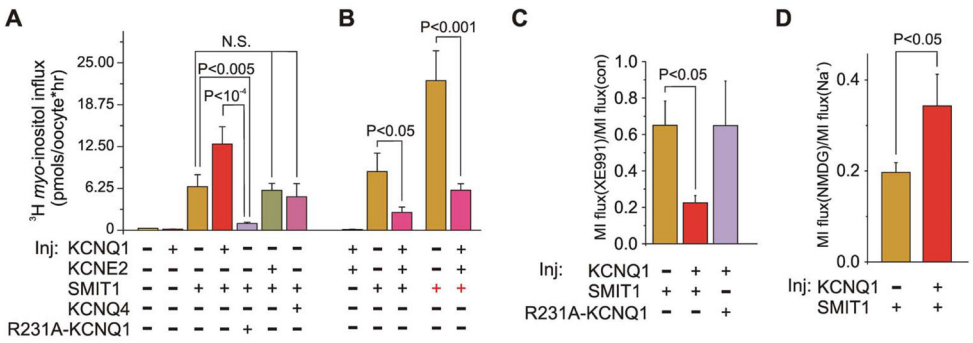

Figure 4. KCNQ1 and KCNQ1-KCNE2 have differential effects on SMIT1 *myo*-inositol transport

A. Mean *myo*-[$^{2\text{-}3}$H(N)] inositol uptake by oocytes injected with cRNA encoding KCNQ1, KCNE2, SMIT1, KCNQ4, and/or R231A-KCNQ1 as indicated; n = 9–12. All SMIT1-injected groups gave mean values significantly different from non-SMIT1-injected groups ($P<0.001$). N.S., non-significant ($P>0.05$).

B. Mean *myo*-[$^{2\text{-}3}$H(N)] inositol uptake by oocytes injected with cRNA encoding KCNQ1, KCNE2, and/or SMIT1 as indicated (black +, SMIT1; red +, SMIT1); n = 10–11. All SMIT1-injected groups gave mean values significantly different from the non-SMIT1-injected group ($P<0.001$).

C. Effects of XE991 on *myo*-[$^{2\text{-}3}$H(N)] inositol uptake by oocytes injected with cRNA encoding KCNQ1, R231A-KCNQ1, and/or SMIT1 as indicated, normalized to mean flux in the absence of XE991 (con); n = 9–12.

D. Effects of Na^+ substitution with NMDG on mean *myo*-[$^{2\text{-}3}$H(N)] inositol uptake by oocytes injected with cRNA encoding KCNQ1, and/or SMIT1 as indicated, normalized to mean flux in the presence of 96 mM NaCl (con); n = 12–13.

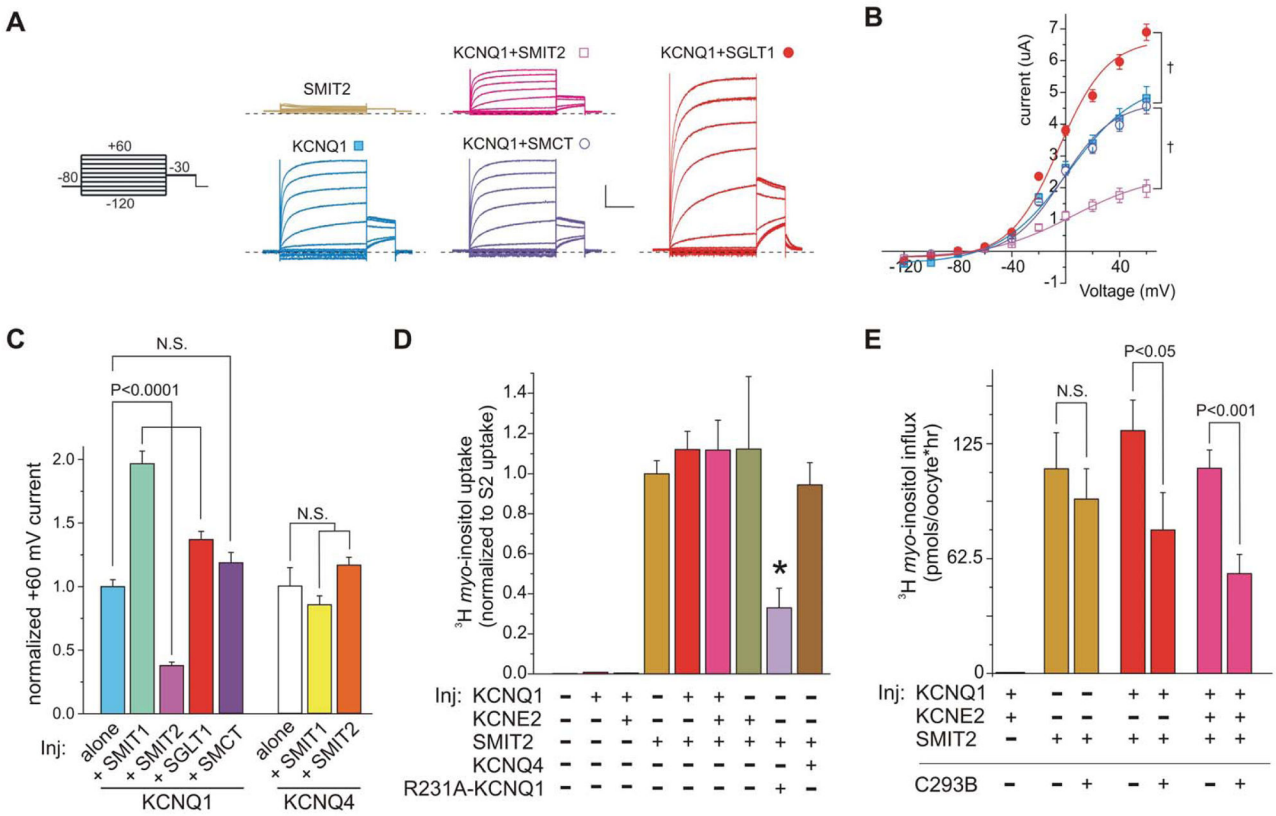

Figure 5. Co-regulation of the KCNQ1 channel with SMIT2 and SGLT1 transporters

A. Exemplar current traces recorded in oocytes expressing KCNQ1 and/or SMIT2, SMCT, SGLT1, using the standard voltage family protocol (inset). Scale bars: vertical, 1 μA; horizontal, 1 s. Zero current levels indicated by dashed lines.

B. Mean raw current-voltage relationships, oocytes (and symbols) as in (A); *n* = 19 (KCNQ1), 13 (SMIT2+KCNQ1), 12 (SMCT+KCNQ1), 16 (SGLT1+KCNQ1). † P<0.0001 at 60 mV.

C. Mean effects of the various transporters on KCNQ1 or KCNQ4 current density at 60 mV normalized to current density in the absence of co-expressed transporters, pooled from 2–3 batches of oocytes; *n* = 25–37. N.S., non-significant (P>0.05).

D. Mean *myo*-[$^{2\text{-}3}$H(N)] inositol uptake of oocytes injected with cRNA encoding KCNQ1, KCNE2, SMIT2, KCNQ4, and/or R231A-KCNQ1 as indicated. Data are pooled from 4–5 batches of oocytes and normalized to each intra-batch mean for SMIT2 alone (*n* = 45–51) except for KCNQ4 and R231A-KCNQ1 (each pooled and normalized from 2 batches, *n* = 16–19).

E. Mean *myo*-[$^{2\text{-}3}$H(N)] inositol uptake by oocytes injected with cRNA encoding KCNQ1, KCNE2, and/or SMIT2 as indicated; *n* = 9–10.